Scattering of High-Energy Electrons from Ca^{40}, V^{51}, Co^{59}, In^{115}, $Sb^{121,123}$, and Bi^{209}†

H. CRANNELL, R. HELM, H. KENDALL, J. OESER, AND M. YEARIAN*
Department of Physics and High-Energy Physics Laboratory, Stanford University, Stanford, California
(Received August 22, 1960)

The absolute elastic electron-scattering cross sections of Ca^{40}, V^{51}, Co^{59}, In^{115}, $Sb^{121,123}$, and Bi^{209} have been measured at a number of angles at a primary electron energy of 183 Mev. The cross sections were obtained by comparison with scattering from the proton. These data have been compared with the previous relative angular distributions measured by Hahn, Ravenhall, and Hofstadter. The present data are in closer agreement with the charge distributions found from fitting a Fermi two-parameter model to the older data than with those found from a fit of the Ford and Hill charge distributions. The absolute cross sections for Bi^{209} show the least agreement: they are 35% larger than the predictions of the Fermi model and about 70% larger than the Ford and Hill model.

I. INTRODUCTION

In the past few years, considerable attention has been given to the determination of nuclear sizes using the techniques of high-energy electron scattering.[1] A number of medium- and high-Z nuclei were investigated by Hahn, Ravenhall, and Hofstadter[2] (referred to hereafter as HRH). HRH measured relative differential elastic scattering cross sections for a number of nuclei as a function of laboratory angle. These measurements were compared with the scattering predicted by the phase-shift calculations of Yennie *et al.*[3] HRH used a nuclear charge density $\rho(r)$ given by the Fermi two-parameter model,

$$\rho(r)=\frac{\rho_0}{1+\exp[(r-c)/z_1]}, \tag{1}$$

where c is the radius at which the charge density falls to one half its maximum value, and z_1 is the surface-thickness parameter; the radial variable r is measured from the center of the nucleus.

A more familiar nuclear surface-thickness parameter t is defined[1] as the distance in which the charge density drops from 90% to 10% of its maximum value. For the charge distribution described by Eq. (1), $t=4.4z_1$ if c is much larger than z_1. The relative angular distributions were used to determine c and z, although there remained some uncertainty as the absolute cross sections were not available. HRH used other models with parameters which could be adjusted to fit the predicted scattering to the data. The best values of the radial and skin-thickness parameters are model dependent, as are the absolute cross sections predicted on the basis of the best fit to the observed angular distributions.

The Fermi charge distribution gives a rather simple relation for the variation of c with atomic number, $c\cong 1.07A^{\frac{1}{3}}$; t has the approximately constant value 2.5 f.

Recently, Ford and Hill[4] have proposed a model which they have used in making an extensive analysis of the HRH angular distributions; it is known as the "Family II" model. The nuclear charge distribution is given by

$$\rho(r)=\frac{\rho_1}{1-\frac{1}{2}e^{-n}}\times\begin{cases}1-\frac{1}{2}e^{-n(1-X)}; & X\leqq 1,\\ \frac{1}{2}e^{-n(X-1)}; & X\geqq 1,\end{cases} \tag{2}$$

where $X\cong r/c$ and n is a continuously varying parameter related to c/t. For $n=0$, $\rho(r)$ becomes an exponential charge distribution.[1] For $n\to\infty$, $\rho(r)$ approaches a uniform model. In the region $4\leqq n\cong 10$, $\rho(r)$ is similar to the Fermi model.

The fits to the HRH data obtained by Ford and Hill yield somewhat different values of c and t and absolute cross sections varying from 0.5 to 0.85 of the values predicted by the Fermi model.

Table I shows the results of Ford and Hill's calculations using the Family II model in comparison with the work of HRH. Values of c, t, and n are given as well as the ratio of the absolute cross sections predicted by Ford and Hill and by HRH.

In the present work we have measured a number of absolute scattering cross sections at the experimental parameters selected by HRH, in order to remove the ambiguities in the absolute cross sections determined by them by fitting the data to relative angular distributions. The present data reduce the uncertainty of the model fitting and provide more stringent criteria for the selection of a model. We have used targets of Ca^{40}, V^{51}, Co^{59}, In^{115}, $Sb^{121,123}$, and Bi^{209}, bombarded by 183-Mev electrons, measuring the absolute differential scattering cross sections at a number of angles in the range 40°–90°. The experimental parameters chosen are those of

† Supported by the joint program of the Office of Naval Research, the U. S. Atomic Energy Commission, and the Air Force Office of Scientific Research.
* Now at the University of Pennsylvania, Philadelphia, Pennsylvania.
[1] For reviews of the experimental and theoretical situation before 1957, see R. Hofstadter, Revs. Modern Phys. **28**, 214 (1956), and *Annual Review of Nuclear Science* (Annual Reviews, Inc., Palo Alto, California, 1957), Vol. 7, p. 231.
[2] B. Hahn, D. G. Ravenhall, and R. Hofstadter, Phys. Rev. **101**, 1131 (1956).
[3] D. R. Yennie, R. N. Wilson, and D. G. Ravenhall, Phys. Rev. **92**, 1325 (1953); D. R. Yennie, D. G. Ravenhall, and R. N. Wilson, Phys. Rev. **95**, 500 (1954).
[4] K. W. Ford and D. L. Hill, *Annual Reviews of Nuclear Science* (Annual Reviews, Inc., Palo Alto, California, 1955), Vol. 5, p. 25, see also D. L. Hill, in *Handbuch der Physik*, edited by S. Flügge (Springer-Verlag, Berlin, Germany, 1957), Vol. 39, p. 178.

TABLE I. Parameters of the two solutions.

Element	Ford and Hill (Family II) c (fermi)	$c/A^{\frac{1}{3}}$	t (fermi)	n	HRH (Fermi) c (fermi)	$c/A^{\frac{1}{3}}$	t (fermi)	n	σ_{II}/σ_{HRH}
Ca^{40}	3.638	1.063	2.80	4.1	3.64	1.063	2.5	4.6	0.6 ±0.1
V^{51}	3.920	1.057	2.50	5.0	3.98	1.073	2.2	5.8	0.7 ±0.03
Co^{59}	4.096	1.052	3.05	4.25	4.09	1.051	2.5	5.2	0.5 ±0.08
In^{115}	5.251	1.080	2.25	7.5	5.24	1.078	2.3	7.3	0.85±0.1
$Sb^{121,123}$	5.370	1.083	2.38	7.25	5.32	1.073	2.5	6.8	0.85±0.08
Bi^{209}	6.493	1.094	2.79	7.5	6.47	1.090	2.7	7.7	0.80±0.04

HRH and were selected so as to allow direct comparison with the cross sections predicted by the Fermi and Family II models.

II. APPARATUS AND PROCEDURE

The experimental apparatus used in the experiments has been described.[1] The single-channel detector used with the 36-in. magnetic spectrometer was replaced by a multichannel detector that allowed simultaneous collection of data at ten different values of electron momenta. The momentum acceptance Δp of each channel was determined by the relation $\Delta p/p \cong 0.3\%$, where p is the final momentum of the scattered electrons. This multiple detector is similar to that described by Kendall.[5] The liquid-filled Čerenkov counter described by Kendall[5] was replaced by one using a Lucite radiator, and DuMont K1382 end-window photomultipliers replaced the 931 type photomultipliers used previously to view the small scintillators.

This multichannel device has not been used in previous experiments, and because the methods of taking data differ from those used with the older single-channel detector, we will give a brief description of the techniques employed.

All of the nuclei we have studied here, except Ca^{40} and In^{115}, have excited states of about 1-Mev excitation. The momentum resolution employed in the experiment needed to be high enough so that scattered electrons which excited the target nucleus to its first excited state could be distinguished from elastically scattered electrons. For the present experiment $\Delta p/p \leqq 0.45\%$, where Δp is the full width at half-maximum of the momentum resolution function.

Each data-taking run was preceded and succeeded by calibration runs to determine the counting efficiency of each channel, using the peak region of the continuous inelastic spectrum of electrons scattered from C^{12}. This spectrum is nearly flat over a 3% momentum interval centered at its peak. Accumulating 500 to 2000 counts per channel was sufficient to allow the determination of the relative efficiency of each channel and to determine drifts in the operating points of parts of the equipment. A number of such calibration runs resulted in a total of $\sim 10^4$ counts per channel from which the efficiencies could be determined to satisfactory accuracy. We rejected data from channels whose efficiencies varied beyond what was expected from normal statistical counting fluctuations. The scattering data were cor-

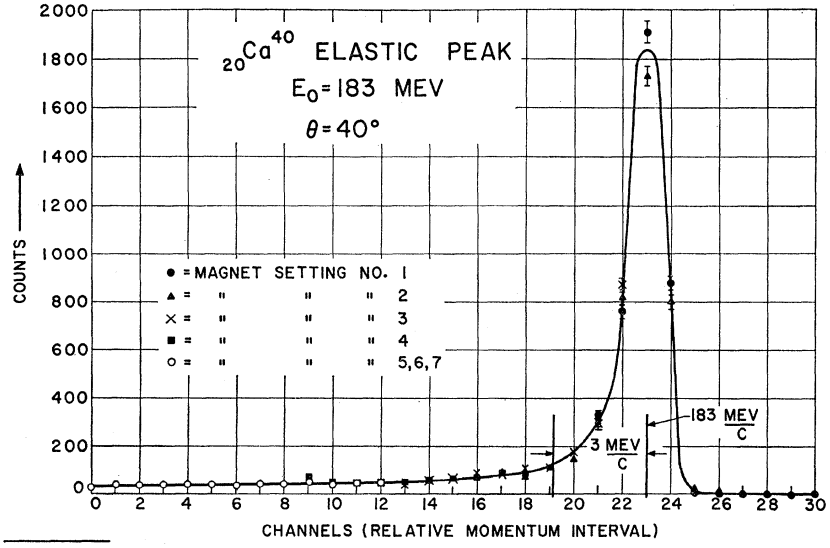

FIG. 1. The Ca elastic peak at 40°. There are ten data points for each magnet setting ("exposure") and there are seven settings. The abscissa is the channel number (arbitrary) and proportional to the electron energy. Some momenta are marked for reference. The long vertical grid lines are two channels apart; each channel defines a Δp of $0.003p$. The channels have all been normalized to the same efficiency.

[5] H. W. Kendall, Trans. Inst. Radio Engrs. NS-5, 190 (1958).

rected for the different efficiencies of the various channels.

The number of channels was large enough to display an entire elastic peak profile at once. The counters in the detector array were placed close together, so that the number of detected electrons, and hence the differential cross section, was proportional to the integral of the peak profile without the application of the dispersion correction usual in single-channel detection.[1]

With the exception of the Co^{59} and Ca^{40} targets, we used the same targets as HRH. The Co^{59} target was made from the same stock as in the earlier experiments but was milled to 0.014 in. thickness from the 0.042 in. used previously. The Ca^{40} target was prepared at Stanford Research Institute by heating commercial-

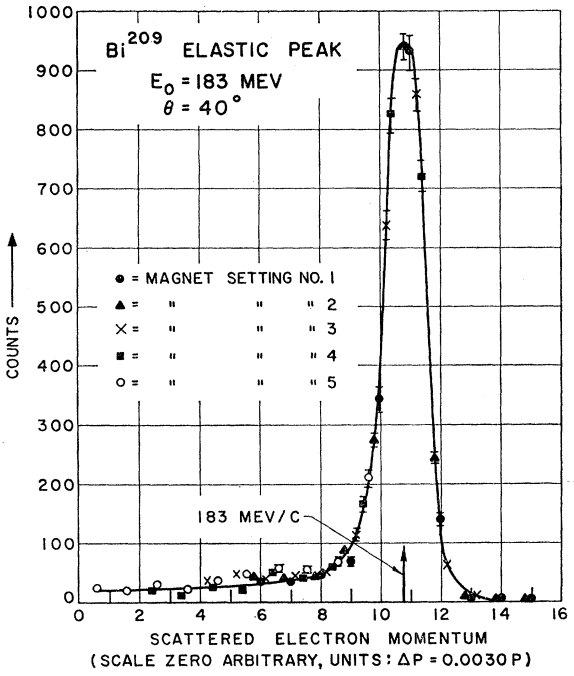

FIG. 2. The Bi elastic peak at 40°.

grade calcium chips and molding under an argon atmosphere. The final thickness of 0.090 in. was achieved by milling under kerosene. The target contained 96% Ca^{40}. It was stored in diffusion pump oil to retard oxidation of the surface. Approximately 1% oxygen was observed in the scattering experiments. Because of recoil of the target nucleus, the elastic peak from oxygen lies about 0.7% lower in momentum than the peak from Ca^{40}, and the yield of electrons scattered from oxygen could be identified and subtracted.

The targets used were thin enough so that multiple scattering and straggling could not cause part of the beam to miss either the secondary emission monitor or the Faraday cup which were used to integrate the primary electron beam.[2]

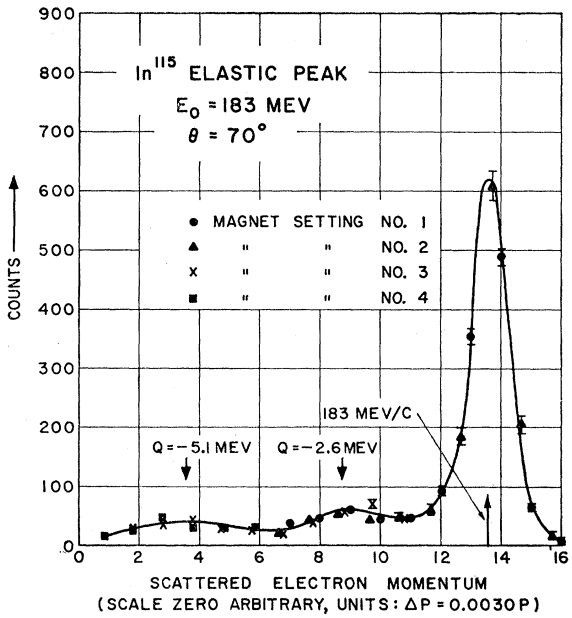

FIG. 3. The In elastic peak at 70°.

Figures 1, 2, and 3 show typical elastic scattering peaks corrected for the variation in efficiency of the separate channels. Each peak contained data from three or more runs at slightly different spectrometer magnetic field settings to define the profile more accurately and to show any irregularities in the application of the channel efficiency corrections.

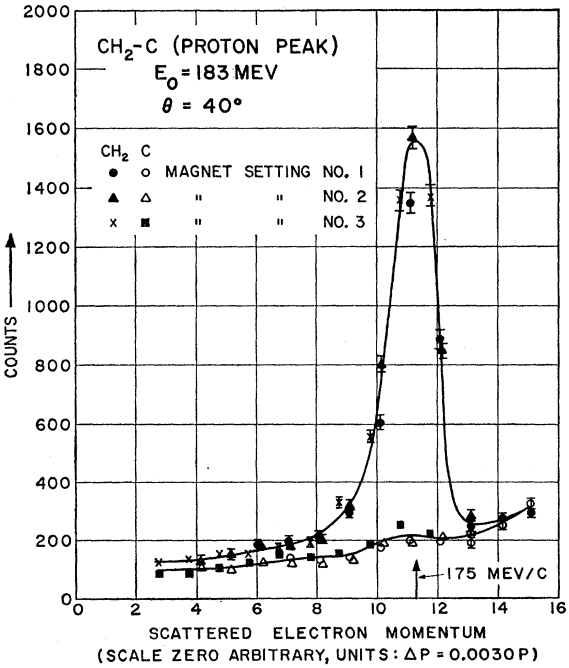

FIG. 4. The curves from the matched CH_2 and C^{12} targets at 40°. The proton peak is obtained by subtracting the two curves.

TABLE II. Absolute cross sections.

(1) Element	(2) θ	(3) σ_{II}/σ_{HRH}	(4) $\sigma(\theta)_{HRH}$ (cm²/sr)	(5) $\sigma(\theta)_{exp}$ (cm²/sr)	(6) $\sigma_{exp}/\sigma_{HRH}$	(7) $\langle\sigma_{exp}/\sigma_{HRH}\rangle_{av}$
Ca^{40}	40°	0.6 ±0.1	7.6×10^{-28}	$(5.53 \pm 0.55) \times 10^{-28}$	0.73 ±0.07	
	50°		9.3×10^{-29}	$(7.66 \pm 0.14) \times 10^{-29}$	0.825±0.015	
	70°		5.9×10^{-31}	$(8.06 \pm 0.8) \times 10^{-31}$	1.37 ±0.14	
	70°		5.9×10^{-31}	$(7.33 \pm 0.7) \times 10^{-31}$	1.24 ±0.12	
	85°		2.45×10^{-31}	$(2.62 \pm 0.09) \times 10^{-31}$	1.07 ±0.04	1.047±0.040
V^{51}	45°	0.7 ±0.03	2.6×10^{-28}	$(2.53 \pm 0.25) \times 10^{-28}$	0.97 ±0.10	
	70°		8.4×10^{-31}	$(9.81 \pm 0.98) \times 10^{-31}$	1.17 ±0.12	
	80°		8.1×10^{-31}	$(8.17 \pm 0.28) \times 10^{-31}$	1.01 ±0.04	1.050±0.053
Co^{59}	40°	0.5 ±0.08	8.0×10^{-28}	$(8.06 \pm 0.81) \times 10^{-28}$	1.01 ±0.10	
	45°		2.47×10^{-28}	$(2.36 \pm 0.24) \times 10^{-28}$	0.96 ±0.10	
	60°		4.90×10^{-30}	$(5.18 \pm 0.16) \times 10^{-30}$	1.06 ±0.03	
	70°		1.57×10^{-30}	$(1.625 \pm 0.16) \times 10^{-30}$	1.03 ±0.10	
	70°		1.57×10^{-30}	$(1.92 \pm 0.19) \times 10^{-30}$	1.22 ±0.12	
	75°		1.39×10^{-30}	$(1.86 \pm 0.08) \times 10^{-30}$	1.34 ±0.06	
	75°		1.39×10^{-30}	$(1.69 \pm 0.06) \times 10^{-30}$	1.22 ±0.05	
	100°		1.42×10^{-31}	$(1.58 \pm 0.10) \times 10^{-31}$	1.11 ±0.07	1.118±0.030
In^{115}	40°	0.85±0.1	1.02×10^{-27}	$(9.24 \pm 0.92) \times 10^{-27}$	0.91 ±0.09	
	70°		0.99×10^{-29}	$(1.02 \pm 0.10) \times 10^{-29}$	1.01 ±0.10	
	100°		1.46×10^{-31}	$(1.51 \pm 0.14) \times 10^{-31}$	1.03 ±0.10	0.982±0.056
$Sb^{121,123}$	40°	0.85±0.08	9.2×10^{-28}	$(8.02 \pm 0.8) \times 10^{-28}$	0.87 ±0.09	
	70°		9.1×10^{-30}	$(9.1 \pm 0.91) \times 10^{-30}$	1.00 ±0.10	
	70°		9.1×10^{-30}	$(8.5 \pm 0.85) \times 10^{-30}$	0.93 ±0.09	0.933±0.054
Bi^{209}	40°	0.80±0.04	2.15×10^{-27}	$(2.48 \pm 0.25) \times 10^{-27}$	1.15 ±0.12	
	50°		3.97×10^{-28}	$(4.01 \pm 0.12) \times 10^{-28}$	1.01 ±0.03	
	55°		1.65×10^{-28}	$(2.34 \pm 0.08) \times 10^{-28}$	1.42 ±0.05	
	60°		5.2×10^{-29}	$(7.86 \pm 0.21) \times 10^{-29}$	1.51 ±0.04	
	65°		1.65×10^{-29}	$(2.33 \pm 0.08) \times 10^{-29}$	1.41 ±0.05	
	65°		1.65×10^{-29}	$(2.05 \pm 0.17) \times 10^{-29}$	1.24 ±0.10	
	70°		7.0×10^{-30}	$(10.96 \pm 0.33) \times 10^{-30}$	1.56 ±0.05	
	70°		7.0×10^{-30}	$(9.97 \pm 0.99) \times 10^{-30}$	1.42 ±0.14	
	70°		7.0×10^{-30}	$(9.00 \pm 0.90) \times 10^{-30}$	1.29 ±0.13	
	75°		4.75×10^{-30}	$(6.76 \pm 0.28) \times 10^{-30}$	1.42 ±0.06	
	75°		4.75×10^{-30}	$(6.55 \pm 0.32) \times 10^{-30}$	1.38 ±0.07	1.346±0.026

The absolute cross sections have been determined for these and the other peaks by comparison with elastic scattering from the protons in a polyethylene target. A carbon target having the same number of carbon nuclei per cm² as the polyethylene was used to determine the carbon background (see Fig. 4). The absolute cross sections for electron scattering from the proton have been measured.[6,7] Several proton peaks were taken during each run, usually at several angles to ensure that the detection efficiency did not depend on the spectrometer field setting.

III. TREATMENT OF THE DATA

The data were corrected for the efficiencies of the channels, as discussed above, and plotted. The area under the peaks was determined by graphical or numerical methods. The integrations were carried to a momentum Δp lower than the momentum of the maximum of each peak. The value of Δp was chosen to be greater than the width w of each peak at half-amplitude; Δp was $\geqq 0.004p$ for the data runs and was $\geqq 0.007p$ for the proton calibration runs. Bremsstrahlung and Schwinger corrections were applied to these peak areas.[1] The data were normalized to correspond to a standard number of target nuclei per cm² for a standard integrated primary electron beam. From these data and the absolute proton cross sections the desired absolute cross sections were determined.

IV. RESULTS

The data of the present experiment and comparisons with theoretical predictions are presented in Table II. For each element are listed the laboratory scattering angles, the ratio of the absolute differential cross sections as predicted from the Family II model σ_{II} and the Fermi model σ_{HRH}, the absolute differential cross sections as predicted by the Fermi model, and the observed differential cross sections $\sigma_{exp}/\sigma_{HRH}$. Averages of $\sigma_{exp}/\sigma_{HRH}$ over the range of the data for each element are given.

Figures 5–8 show some of the experimental and theo-

[6] E. E. Chambers and R. Hofstadter, Phys. Rev. **105**, 1454 (1956).

[7] R. Hofstadter, F. Bumiller, and M. R. Yearian, Revs. Modern Phys. **30**, 482 (1958); and F. Bumiller (private communication).

retical angular distributions and the absolute differential cross sections from Table II. Figure 5 shows several theoretical angular distributions for the scattering from Co^{59}. All of these curves give satisfactory fits to the relative angular distributions of HRH. Curve c is the best fit of this type. The Fermi two-parameter model fits the absolute cross sections most accurately. For this fit, $c=4.09$ f and $t=2.5$ f.

Figure 6 shows similar results for Ca^{40}. The dashed curve is the best fit and is again a Fermi two-parameter model with $c=3.64$ f, $t=2.50$ f. The solid curve is a Family II fit of the angular distribution but with the incorrect absolute cross sections. The middle curve, calculated by U. Meyer-Berkhout,[8] uses the parameters of the Ford and Hill model in the Fermi model; it is incorrect in both angular distribution and absolute cross section.

Figure 7 shows the data for V^{51} and the agreement between the data and the HRH fit of the Fermi model.

Figure 8 shows a similar curve for Bi^{209}. The data at the larger angles are consistently about 35% above the earlier best fit by HRH using the Fermi model. Table I shows that the agreement with the Family II predictions is even worse.

The data fit the predictions of the Fermi two-

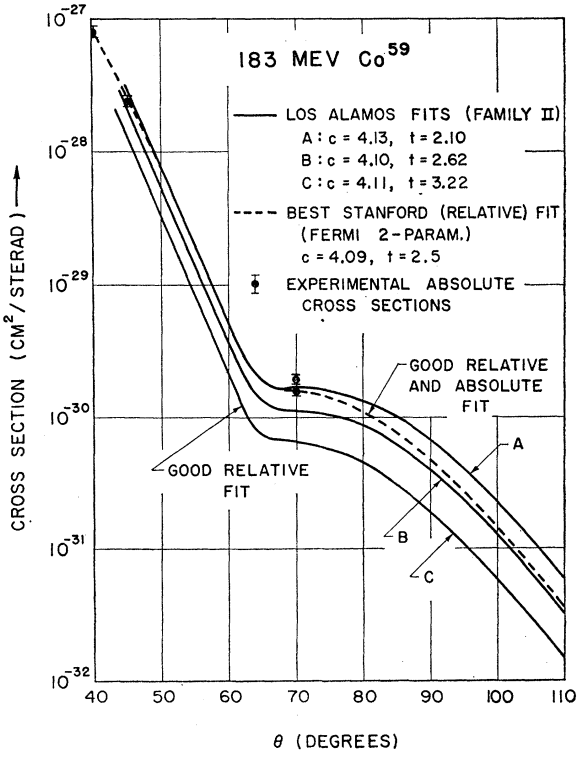

FIG. 5. The angular distributions and cross sections for Co^{59}. The dashed curve is the HRH best fit curve. The curve labeled C is the Family II best fit curve. The two curves have the same relative shape but the cross sections differ by a factor of two. The experimental points favor the HRH (dashed) curve, as described in the text.

[8] U. Meyer-Berkhout, K. W. Ford, and A. E. S. Green, Ann. Phys. 8, 119 (1959).

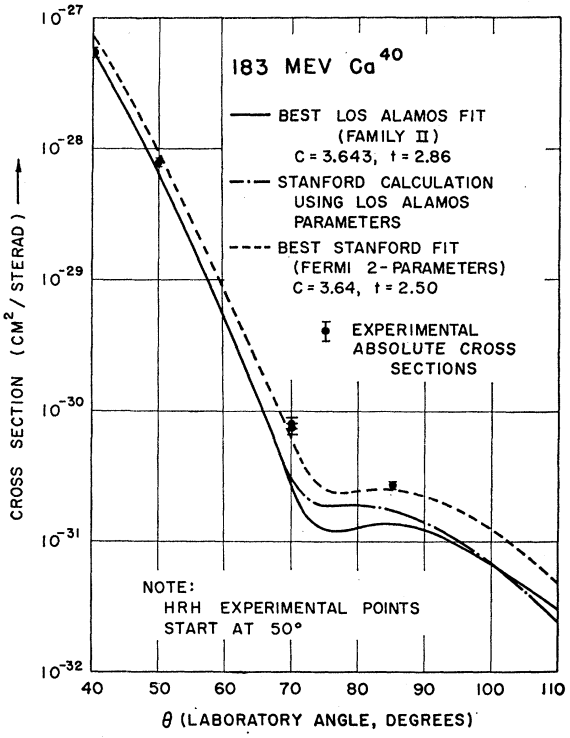

FIG. 6. The angular distributions and cross sections for Ca^{40}. This plot is similar to Fig. 5. Again, the experimental points agree with the HRH solution (see text).

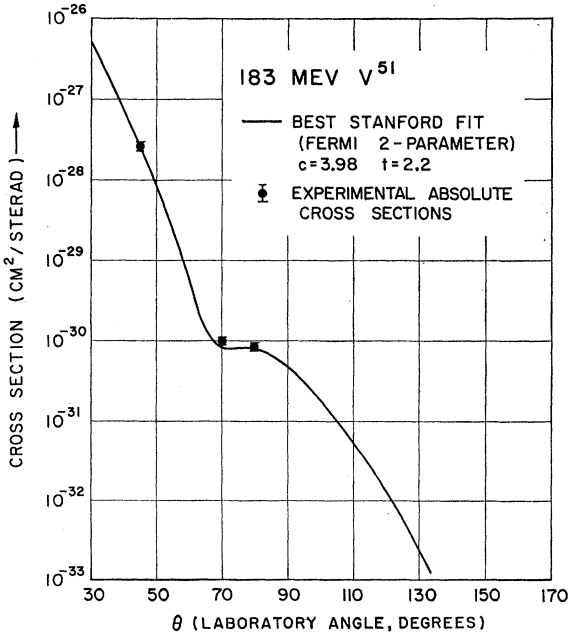

FIG. 7. The angular distribution and cross sections for V^{51}. The solid curve is the HRH solution and is in excellent agreement with the experimental cross sections.

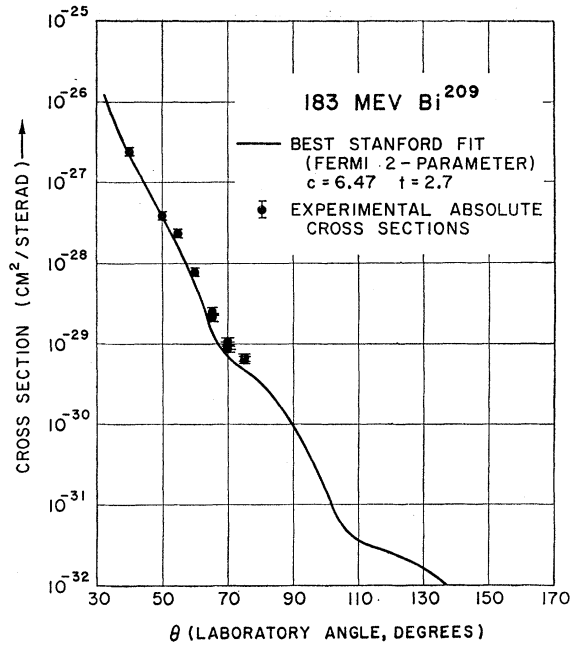

FIG. 8. The angular distribution and cross sections for Bi^{209}. This is the only case for which the Fermi model does not predict the correct cross sections. The experimental values are about 35% too high.

parameter model better than those of the Family II. With the exception of Bi^{209} the agreement is surprisingly good considering that the absolute cross sections remained free parameters in the original determinations of the parameters.

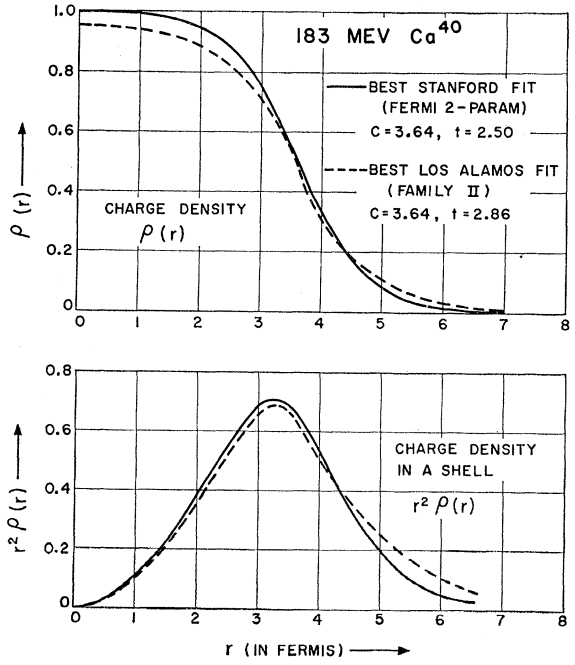

FIG. 9. The charge density $\rho(r)$ and $r^2\rho(r)$ for the two models for Ca^{40}. The charge densities appear to be similar, but there is more charge at large values of r for the Family II solution.

Figure 9 shows the charge densities $\rho(r)$ and the charge density in a shell $r^2\rho(r)$ predicted for Ca^{40} by the two models. The Family II model predicts slightly more charge at larger radii than the Fermi model.

The errors shown in Table II and in Figs. 5–8 are the standard deviations arising from counting statistics only in the determinations of the target-nuclei elastic peak areas and of the proton calibration peaks. No errors from the measurements of HRH are included, nor are their errors in the fitting of their data to the angular distributions.

Shifts in the parameters of a cross-section determination (e.g., electron beam spot position, fluctuations in analyzing magnet current) introduce a lack of reproducibility in experimental determinations of the cross sections. The data presented here were reproducible to no better than 10% for repeated runs at the same target and target angle when the statistical errors were of the order of 2–3%.

The accuracy of the determinations of the density of target nuclei was estimated to be from 2% to 3%.

We have assigned errors of 7–10% to the ratios $\sigma_{\text{exp}}/\sigma_{\text{HRH}}$ given in column (7) of Table II, depending on the number of data points measured for the particular element. Thus, for all the nuclei except Bi^{209}, the quantity $\sigma_{\text{exp}}/\sigma_{\text{HRH}}$ is unity within experimental error.

The main conclusion of the experiment, then, is that for Ca, V, Co, In, and Sb, the analysis of the angular distribution alone using the Fermi two-parameter model also predicts the correct absolute cross sections within about 10%. In particular, in all cases (including Bi^{209}) the Family II model predicts cross sections which are significantly too low. That the Fermi model predicts the correct cross sections is quite surprising since there was really no *a priori* reason for its choice by HRH as the prototype model for the charge density.

In the case of Bi, the Fermi model appears to give cross sections that are too low by perhaps 35%. There is no reason known for this. It appears to indicate that for Bi^{209} the surface thickness is much smaller relative to the rms radius than for the lighter nuclei, and it might be that the Fermi model is not general enough to be used successfully in analysing the scattering from heavy nuclei. We have tried using the Fermi three-parameter model to see if these high cross sections might be an indication that a model with a central depression is needed. This model can be written:

$$\rho=\frac{\rho_2[1+(wr^2/c^2)]}{1+\exp[(r-c)/z_2]}, \tag{6}$$

where w measures the amount of depression of the central density (at $r=0$). A value of w greater than zero corresponds to a decrease in the central density; for example, $w=+0.64$ corresponds roughly to a 20% depression of the density at the origin. The three-parame-

ter charge distribution reduces to the Fermi two-parameter distribution [Eq. (1)] when w equals zero. The parameter z_2 is related to the surface thickness, but no simple relation can be given with the 90%–10% fall-off distance. We find a whole range of values of w for which we can reproduce the curve for the Fermi two-parameter case; however, we have not found a combination of parameters which will raise the cross sections by 35%. The Bi question, therefore, has not been resolved, and more analysis is necessary to determine a model to give a better fit to both the angular distribution and the absolute cross sections.

Figure 3 shows, in addition to the elastic scattering peak, peaks from inelastic scattering of electrons from In^{115} with excitation of nuclear levels at about 2.6 and 5.1 Mev. The form factors associated with inelastic scattering with excitation of these levels, and others in Ni^{58}, Ni^{60}, and Pb^{208}, is being studied; some of the results have been reported.[9]

ACKNOWLEDGMENTS

The authors appreciate the support of Professor Robert Hofstadter throughout the course of the experiment. We are indebted to Dr. K. W. Ford and Dr. U. Meyer-Berkhout whose calculations and suggestions prompted this research. Many members of the High-Energy Physics Laboratory staff have contributed to the success of this work, and in particular we wish to acknowledge the technical assistance of L. Buss, C. N. Davey, and M. Ryneveld, and of Professor R. Mozley and the accelerator crew.

[9] H. Crannell, R. Helm, H. W. Kendall, J. Oeser, and M. Yearian, Bull. Am. Phys. Soc. **5**, 270 (1960).

PHYSICAL REVIEW VOLUME 121, NUMBER 1 JANUARY 1, 1961

Effects of the Pion-Pion Resonance and the Three-Pion Resonance or Bound State on Neutral-Pion Decay*†

How-sen Wong‡
Lawrence Radiation Laboratory, University of California, Berkeley, California
(Received July 27, 1960; revised manuscript received September 28, 1960)

We have applied the dispersion method to the problem of neutral-pion decay. It is shown that a pion-pion P-wave resonance can produce a large effect in the decay matrix element. The contribution is related to the semifundamental constant which determines the rate of photoproduction of pions from pions. The contribution of a strong three-pion state is also considered.

RECENTLY Frazer and Fulco[1] and Chew[2] have proposed that a two-pion P-wave resonance and a three-pion resonance or bound state may account for the isotopic vector and scalar components of nucleon electromagnetic structure, respectively. The purpose of this note is to investigate the effects of such resonances on neutral-pion decay.

The dispersion analysis of neutral-pion decay was first considered by Goldberger and Treiman,[3] but they assumed nucleon-antinucleon pairs to be the most important intermediate states and neglected multipion states. Here we adopt a different approach and consider the contributions of the least massive states. This can be done if we extend a photon variable q^2 into the complex plane instead of the meson variable p^2 used by Goldberger and Treiman.

Following the standard method, one has[4] (see Fig. 1)

$$\langle q(\mu),k(\nu)\,|\,T\,|\,p(3)\rangle = \frac{i(2\pi)^4\delta^4(p-q-k)F_\nu(-q^2;-k^2;-p^2)\epsilon_\nu'}{(8q_0k_0p_0)^{\frac{1}{2}}}, \quad (1)$$

where we have

$$F_\nu=(4p_0q_0)^{\frac{1}{2}}\langle q(\mu)\,|\,J_\nu(0)\,|\,p(3)\rangle,$$

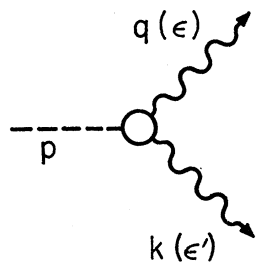

FIG. 1. Neutral-pion decay. Wavy lines are photons; broken line, pion.

* Work done under the auspices of the U. S. Atomic Energy Commission.

† A preliminary account of this work was given at the meeting of the American Physical Society, November 27–28, 1959, Cleveland, Ohio [How-sen Wong, Bull. Am. Phys. Soc. 4, 407 (1959)].

‡ Now at Laboratory of Nuclear Studies, Cornell University, Ithaca, New York.

[1] W. R. Frazer and J. R. Fulco, Phys. Rev. Letters **2**, 365 (1959); Phys. Rev. **117**, 1609 (1960).

[2] G. F. Chew, Phys. Rev. Letters **4**, 142 (1960).

[3] M. L. Goldberger and S. Treiman, Nuovo cimento **9**, 451 (1958).

[4] We use the fundamental metric tensor such that $-p^2=M^2$. Units are used in which $\hbar=c=\mu=1$, where μ is the mass of the pion.